Supporting Information for

Porous metal electrodes enable efficient electrolysis of carbon capture solutions

Zishuai Zhang,[1#] Eric W. Lees,[2#] Faezeh Habibzadeh,[1] Danielle A. Salvatore,[2] Shaoxuan Ren,[1] Grace Simpson,[2] Danika Wheeler,[2] Alyssa Liu,[1] and Curtis P. Berlinguette*[1,2,3,4]

[1]Department of Chemistry, The University of British Columbia, 2036 Main Mall, Vancouver, British Columbia, V6T 1Z1, Canada.

[2]Department of Chemical and Biological Engineering, The University of British Columbia, 2360 East Mall, Vancouver, British Columbia, V6T 1Z3, Canada.

[3]Stewart Blusson Quantum Matter Institute, The University of British Columbia, 2355 East Mall, Vancouver, British Columbia, V6T 1Z4, Canada.

[4]Canadian Institute for Advanced Research (CIFAR), 661 University Avenue, Toronto, M5G 1M1, Ontario, Canada.

[#] These authors contributed to this work equally

*Corresponding author: Curtis P. Berlinguette (cberling@chem.ubc.ca)

Experimental procedures

Methods and Materials

KHCO$_3$ (99.5%, Alfa Aesar, USA), silver nanopowder (~100 nm, 99%, Sigma Aldrich, USA) and ethylenediaminetetraacetic acid, EDTA (99%, Sigma Aldrich, USA) were purchased and used as received. Carbon cloth gas diffusion layers (CeTech® with microporous layer) and Fumasep FBM bipolar membranes were purchased from Fuel Cell Store (USA). The membrane was stored in 1 M NaCl prior to use. Silver foams were obtained from Jiangsu Green Materials Hi-Tech. Co. Ltd. (China). Nickel foams (>99.99%) were purchased from MTI Corporation (USA) and Nafion® 117 solutions (5 wt%; in a mixture of lower aliphatic alcohols and water were obtained from Sigma Aldrich, USA. Nitric acid (70 wt%, Fisher Scientific, USA) was used to make 30% v/v etching solutions.

A CH instrument 660D potentiostat (USA) equipped with an Amp booster was used for all electrolysis experiments. A Ag/AgCl (3 M NaCl) reference electrode (BASi®) was used for electrochemical surface area measurement. A gas chromatography instrument (GC, Perkin Elmer, Clarus 580), equipped with a packed MolSieve 5 Å column and a packed HayeSepD column was used to detect CO and H$_2$ using a flame ionization detector (FID) and a thermal conductivity detector (TCD), respectively. Argon (99.999%, Praxair Canada Inc.) was the carrier gas. The concentrations of the products CO and H$_2$ (ppm) in the headspace of the catholyte reservoir were quantified using previously constructed calibration lines for CO and H$_2$. The spray-coater (Power Fist, China) equipped with a 0.22 mm nozzle and 2 ml paint cup was used for deposition of catalyst inks on the gas diffusion layers.

Scanning electron microscopy (SEM) was performed using a FEI Helios NanoLab 650 dual beam scanning electron microscope with an accelerating voltage of 5.0 keV and a beam current of 50 pA. The X-ray diffraction (XRD) data were obtained with a Bruker D8 Advance diffractometer using Cu K-alpha radiation. Data was collected between 2θ angles of 20° to 80° at a rate of 6° per minute.

Cathode Preparation

The silver foam and nickel foam were cut into desired dimensions (2 × 2 cm) with a blade and washed with acetone and water. The silver foam was treated with dilute nitric acid solution (30% v/v HNO_3) in a 50 ml beaker for 10 s to remove the oxide layer and increase its electrochemical surface area. The etched silver foam was further washed thoroughly with deionized (DI) water, followed by a rinse with 3.0 M $KHCO_3$. The prepared electrode was stored in DI water for further use.

To fabricate carbon composite electrodes, a catalyst ink was prepared by mixing 315 mg silver nanoparticles, 15 ml DI water, 15 ml IPA and 420 µl Nafion® 117 solution. The catalyst ink was then spray-coated on the carbon cloth to make multiple electrodes (geometric area: 4 cm^2) with silver loadings of 3.7 ± 0.1 mg cm^{-2}.

Electrolyte Preparation

3 M fresh $KHCO_3$ solution was prepared before each test in a 500-ml volumetric flask. Prior to use in the flow electrolyser, EDTA was added to the stock solution at a concentration of 0.02 M to prevent electrolyte impurities from electrodeposition on the cathode surface.[1]

Electrochemical surface area (ECSA) measurements:

Cyclic voltammetry (CV) of the carbon composite electrode and foam electrode was performed from -0.6 V to -0.4 V (vs. Ag/AgCl) in 3 M $KHCO_3$ solution at different scan rates ranging from 10 to 100 mV s^{-1}. All electrodes had a geometric area of 1 cm^2. ECSA of silver was calculated as C_{dl}/C_S, where C_{dl} represents double layer capacitance and C_S represents the standard capacitance of a smooth planar surface silver in an aqueous electrolyte.[2,3] Values of C_{dl} were calculated based on the following equation: $i=vC_{dl}$, and the current densities were obtained at -0.5 V vs Ag/AgCl.[4] We plotted the current density (i) as a function of scan rates (v), and then the slope represents C_{dl}. C_S was considered constant for all silver electrodes. Therefore, the measured C_{dl} values are directly proportional to the ECSA. Note that, the C_{dl}

measurement for the carbon composite electrode may include contributions from the gas diffusion layer, however, with the potential extra C_{dl} measured, the calculated silver ECSA of the carbon composite electrode is still significantly lower. Results are shown in Figure S3.

Faradaic Efficiency Calculation

We measured the CO selectivity at constant current densities by quantifying the H_2 and CO concentrations (for calculating mole fraction of CO in the gaseous mixture analyzed, χ) through GC.

The FE of a gaseous product k was determined in accordance with Eq. S1.[5]

$$FE = n_k F \chi_k F_m / I \hspace{4cm} \text{Eq. S1}$$

Where n_k is the number of electrons exchanged, F is Faraday's constant (F = 96,485 C/mol), F_m is the molar flow rate in mol/s, and I is the total current in A. The molar flow rate is derived from the volume flow rate F_v by the relation $F_m = pF_v/RT$, with p being the atmospheric pressure in Pa, R the ideal gas constant of 8.314 J/mol K and T the temperature in K.

CO_2 utilization Calculation

CO_2 utilization was calculated in accordance with Eq. S2. This quantity represents the conversion of *in-situ* generated CO_2 into CO, and therefore, the extent to which the CO is diluted with unreacted CO_2.

$$CO_2 \text{ utilization} = [CO]/([CO] + [CO_2]) \times 100\% \hspace{2cm} \text{Eq. S2}$$

Where [CO] and [CO_2] outlets represent the concentrations of CO and CO_2, respectively, as measured by GC analyses.

Energy Efficiency Calculation

The cathodic cell energy efficiency for CO (EE_{CO}) is calculated according to the Eq. S3[6]

$$EE_{CO} = (E_{CO}/\text{full cell potential}) \times FE_{CO} \hspace{4cm} \text{Eq. S3}$$

Liquid Product Detection

We used ^{1}H NMR spectroscopy to identify the concentrations of formate after 60 min of electrolysis at 20 ℃ and after 30 min electrolysis at 70 ℃. After the electrolysis using the etched foam electrodes, A 500 µL aliquot of the circulated catholyte was transferred to an NMR tube and was mixed with benzene-1,3,5-tricarboxylic acid with known concentrations (10, 50, 100, 500 mM) as the internal standard. A mixture of 100 µL deuterium oxide (D_2O) and 400 µL DI H_2O was added to the contents of the tube. The ^{1}H NMR spectra were collected using a 400 MHz spectrometer (Bruker AV400sp) at RT. Water signal was suppressed using Watergate W5 pulse sequence with double gradient echos.[7] A series of standard solutions with known concentrations of formate were prepared and analyzed by ^{1}H NMR, and a calibration curve was created by plotting the relative signal areas versus concentration of formate. Using this method, we determined the concentration of formate in the catholyte solution and used those values to calculate FE_{fomate}. We found out that the formate faradaic efficiencies in both cases were lower than 1%.

Controlled Temperature Experiments

The temperature of the catholyte reservoir was controlled with a water bath set to 20, 40, 60, or 80 °C. The electrolyser inlet temperatures were measured using in-line resistance temperature detectors (RTDs). The catholyte reservoir was placed in a water bath with increased temperatures (T_{bath}) and was

allowed to reach thermal equilibrium before electrolysis. The temperature of the catholyte entering the flow cell was measured at the inlet of the cathode flow plate (T_{inlet}) to account for heat losses during the transfer of liquid from the reservoir to the flow cell.

Pressurized electrolyser Test Station

A sealed vessel with a volume of 1 gallon was designed to feed high pressure bicarbonate solution into the bicarbonate electrolyser (Figure S8). This vessel had 4 ports which were connected to tubing that carried the liquid inlet, liquid outlet, gas inlet, and gas outlet flows. The electrolyte reservoir was filled with 500 mL of 3.0 M $KHCO_3$ solution and was pressurized by supplying N_2 gas to the gas inlet of the vessel while constricting the outlet gas flow using a pressure regulating valve. The gas flow rate was controlled using a mass flow controller positioned upstream of the reservoir. A pressure relief valve was used to prevent overpressurizing the GC. The pressurized liquid electrolyte was pumped to the electrolyser and continuously recycled to the vessel. Digital pressure indicators positioned at the inlet and outlet of the electrolyser were used to measure the system pressure and pressure drop across the cathode compartment. Gas chromatography measurements were taken after 15 minutes of electrolysis. No liquid products were detected by ${}^1H$ NMR. Therefore, the FE_{CO} and FE_{H2} were normalized to 100% for every experiment. These normalized FE values obtained at 1 atm with our pressurized bicarbonate electrolyser test station matched that of the experiments performed at ambient conditions, which confirms that the normalized values are accurate.

An increase in bicarbonate feedstock pressure, p, decreases the rate of CO_2 mass transfer from the electrolyte into the gas phase, R_{MT,CO_2} (Eq. S4).[8]

$$R_{MT,CO_2} = k_{GL,CO_2} M_{CO_2}\left(c_{CO_2(aq)} - H_{CO_2} p y_{CO_2}\right)$$

Eq. S4

Where H_{CO_2} is the Henry's constant for CO_2, y_{CO_2} is the mass fraction of CO_2 in the gas bubbles, and $c_{CO_2(aq)}$ is the CO_2 concentration in the electrolyte. The gas-to-liquid mass-transfer coefficient of CO_2, k_{GL,CO_2}, is given by Eq. S5:

$$k_{GL,CO_2} = \frac{D_{CO_2(aq)}}{\delta_{TF}}$$ Eq. S5

where $D_{CO_2(aq)}$ is the diffusion coefficient of CO_2 in the liquid electrolyte, and δ_{TF} is the thickness of the thin film of electrolyte on the surface of the electrode.[8]

Bicarbonate equilibrium

$CO_3^{2-}{}_{(aq)} + H_2O_{(l)} \rightleftharpoons HCO_3^-{}_{(aq)} + OH^-{}_{(aq)}$, $K_b = 2.0 \times 10^{-4}$ Eq. S6

$HCO_3^-{}_{(aq)} + H_2O_{(l)} \rightleftharpoons H_2CO_{3\,(aq)} + OH^-{}_{(aq)}$, $K_b = 2.5 \times 10^{-8}$ Eq. S7
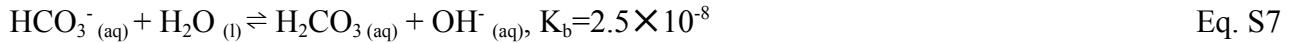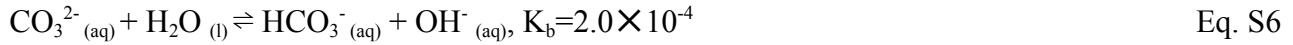
Table S1. The Reported State-of-Art Catalyst Performance for CO_2 Reduction.

Cathode Catalyst	FE_{CO} (%)	Potential (V)	Cell type; Cathode feedstock	Reference
Silver foam electrode	95% at 100 mA cm^{-2};	3.6	"zero-gap" cell; liquid -fed (3 M KHCO$_3$)	This work
Silver composite electrode	82% at 100 mA cm^{-2}	3.4	"zero-gap" cell; liquid -fed (3 M KHCO$_3$)	9
Silver composite electrode	98% at 100 mA cm^{-2}	3.0	"zero-gap" cell; gas -fed (CO$_2$)	10
Silver composite electrode	60% at 50 mA cm^{-2}	-1.5 vs Ag/AgCl (cathode)	"zero-gap" cell; liquid -fed (0.5 M KHCO$_3$ saturateed with CO$_2$)	11
CoPc composite	98% at 150 mA	2.8	"zero-gap" cell;	12

electrode	cm^{-2}		gas -fed (CO$_2$)	
MWNT/PyPBI/Au	98.3% at ~100 mA cm^{-2}	2.5	microfluidic cell; gas -fed (CO$_2$)	13
Silver composite electrode	18% at 104 mA cm^{-2}	4.5-5.5	microfluidic cell; liquid -fed (1.25 M KHCO$_3$)	14
Silver composite electrode	95% at 225 mA cm^{-2} (18.5 atm)	3.7	"zero-gap" cell; liquid -fed (0.5 M K$_2$SO$_4$ saturated with CO$_2$)	15
Unsupported Ag particles	82% at 20 mA cm^{-2}	2.9	microfluidic cell; liquid -fed (0.5 M KHCO$_3$ saturated with CO$_2$)	16
Silver composite electrode	81% at 25 mA cm^{-2}; 33% at 100 mA cm^{-2}	3.4	"zero-gap" cell; liquid -fed (3 M KHCO$_3$)	17

Table S2. Cathodic energy efficiency for CO (EE$_{CO}$) for the electrolyser operated at 4 and 1 atm with the silver foam electrode.

	electrolyser operated at 4 atm	electrolyser operated at 1 atm
FE$_{CO}$ (%)	95	60
Voltage (V)	3.7	3.7
EE$_{CO}$	34%	22%

pristine foam → acid etch → etched foam

50 µm   50 µm
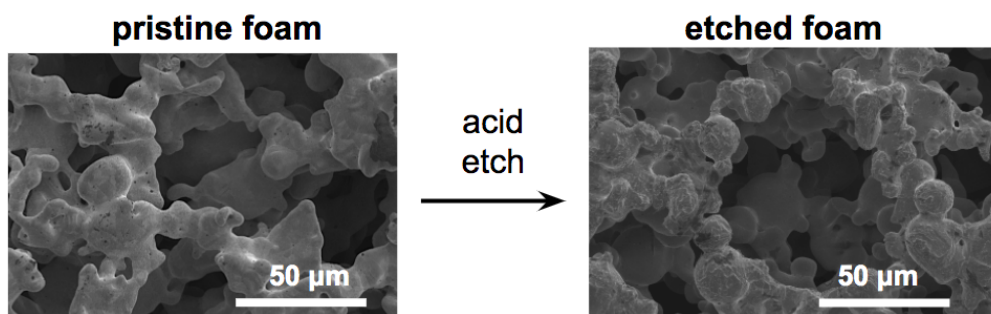
Figure S1. SEM images of the pristine foam and etched foam electrodes under investigation in this work.
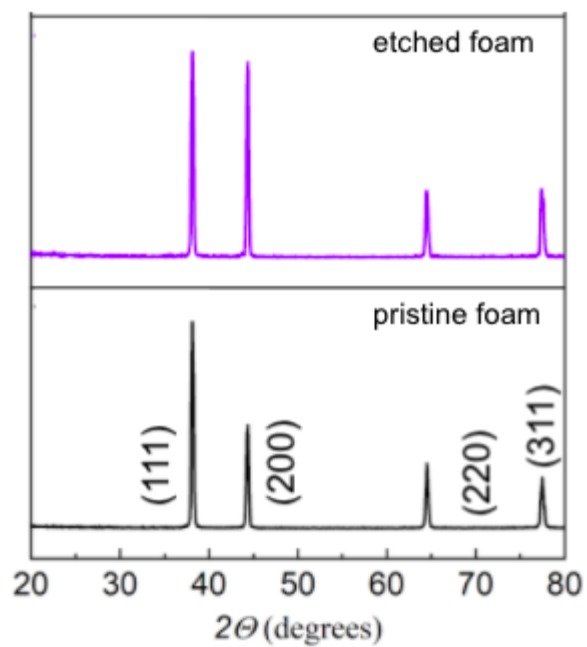
Figure S2. XRD patterns for the pristine foam and etched foam cathodes show no oxide layers were formed during the etching process.[18]
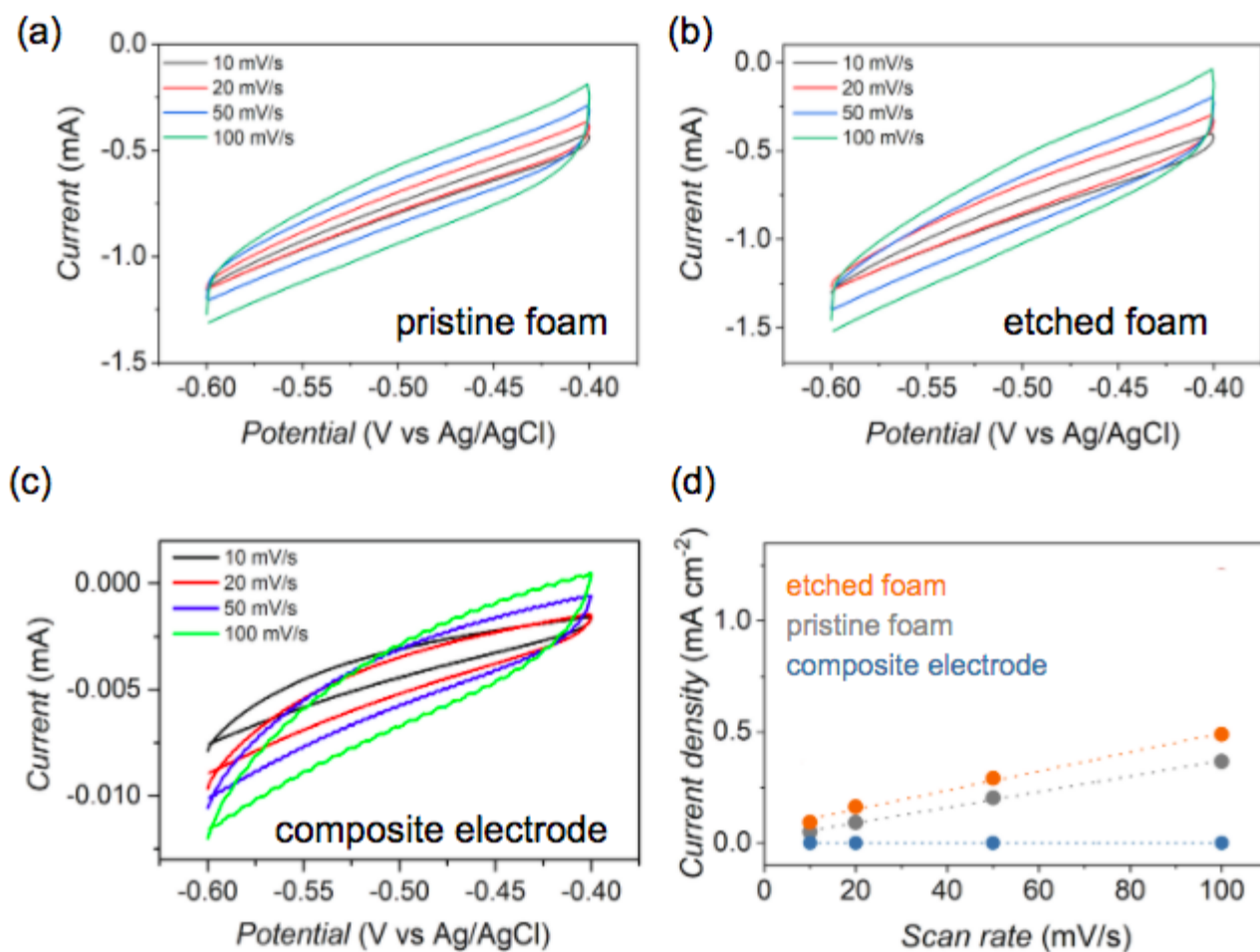
Figure S3. Double layer capacitance measurements used for the determination of the relative electrochemical surface area (ECSA) in non-faradaic regions. (a) Cyclic voltammetry recorded for pristine foam, (b) etched foam and (c) carbon composite electrodes from -0.6 V to -0.4 V (vs. Ag/AgCl). All electrodes had identical geometric surface area of 1 cm^2. We used the current density at -0.50 V (vs. Ag/AgCl) to plot in (d).
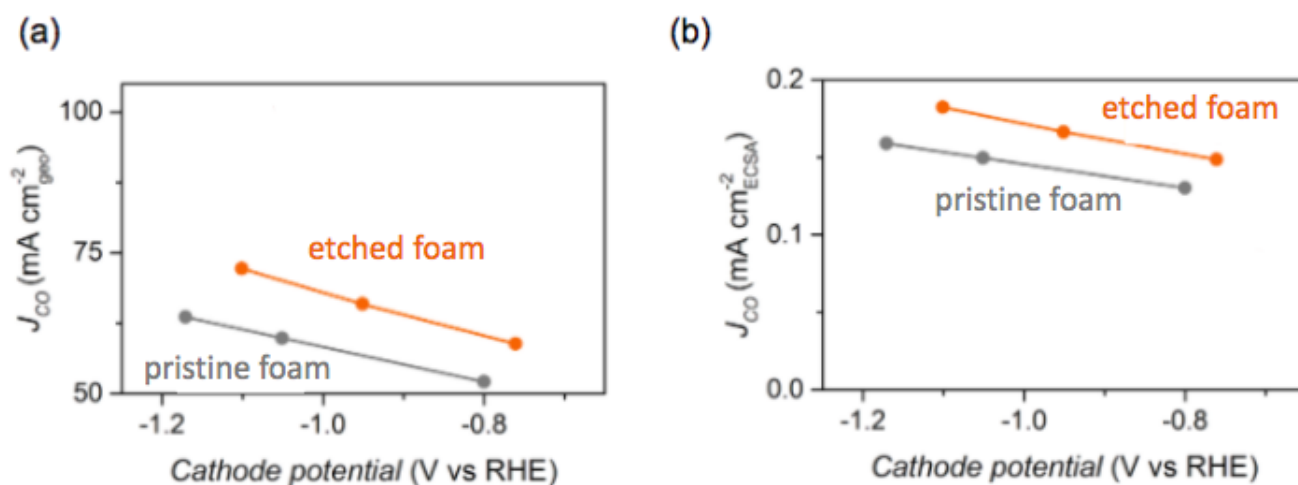
Figure S4. CO partial current density based on the geometric surface area (a) and ECSA (b) with the relationship of the applied cathode potential (RHE scale) for pristine foam and etched foam electrodes.
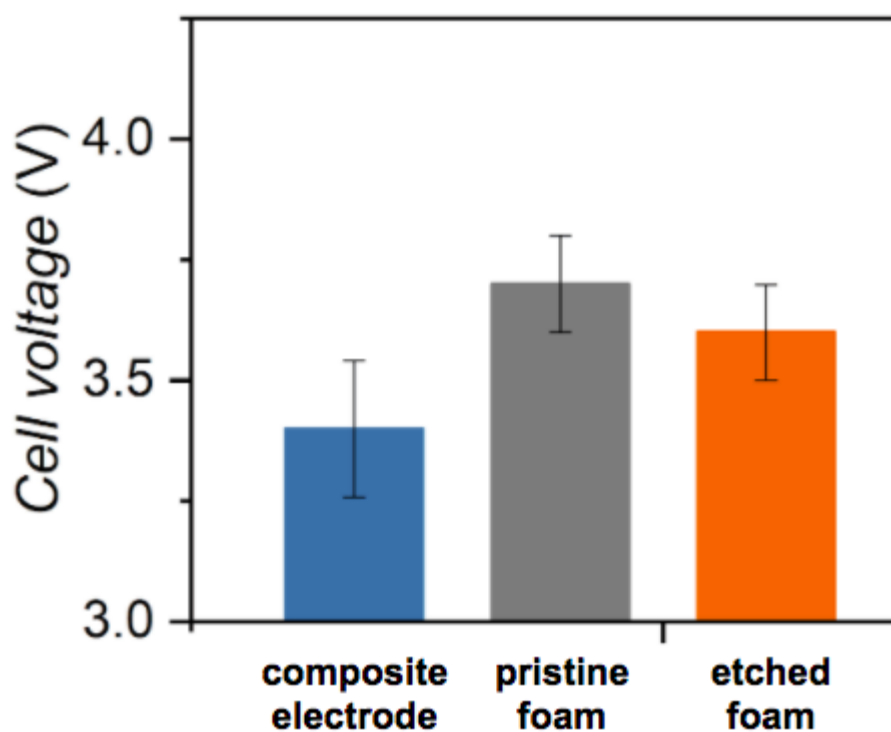
Figure S5. Cell voltages (V_{cell}) obtained with tested cathodes when operating at 100 mA cm^{-2}. Three samples for each cathode were tested, and the data was collected at t=500 s of electrolysis. The uncertainty is the standard deviation of 3 independent measurements.
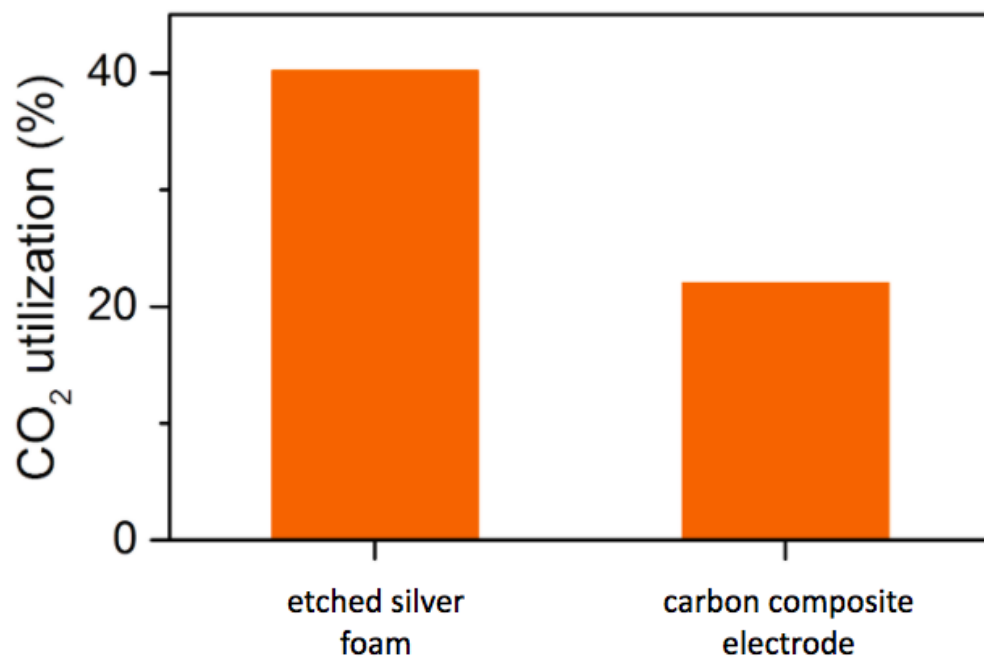
Figure S6. CO$_2$ utilization values for electrolysers containing etched silver foam and carbon composite electrodes at 100 mA cm^{-2}.

(b)

Internal standard

formate

internal standard

EDTA

δ (ppm)
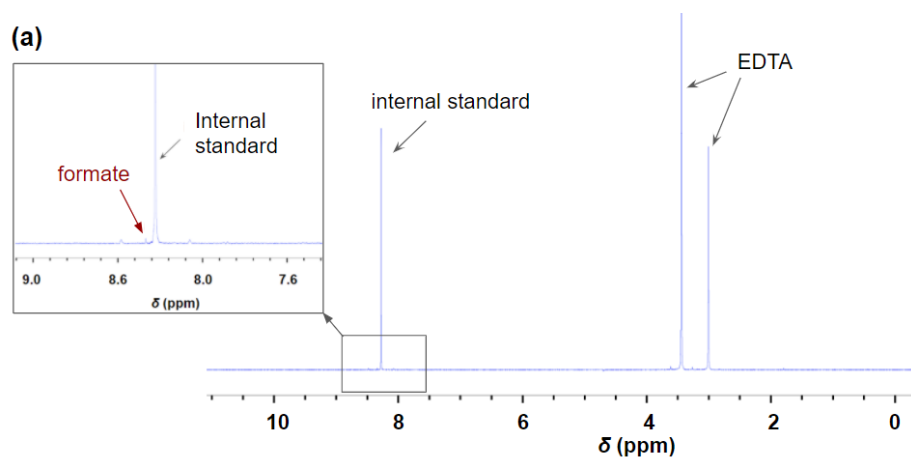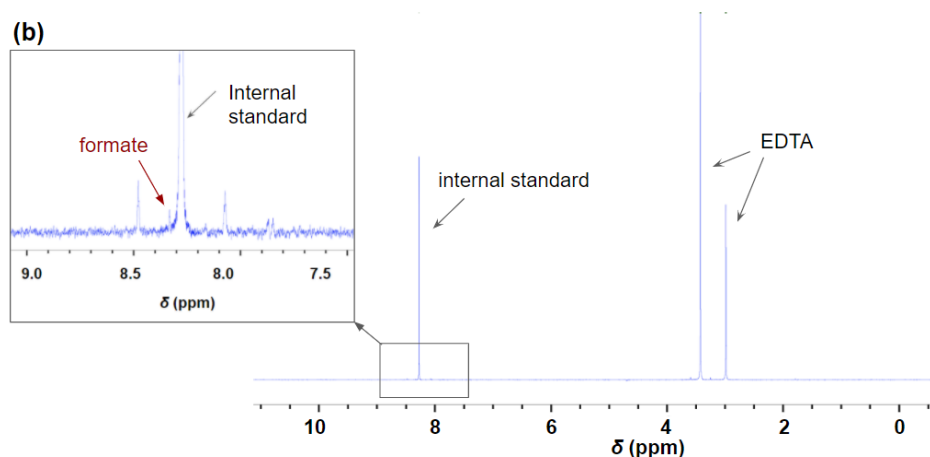
Figure S7: ^{1}H NMR spectra for electrolysis (at 100 mA cm^{-2}) using silver foam electrodes after a) 60 mins at room temperature, and b) 30 mins at 70 ℃. The insets show the area where the formate appears.
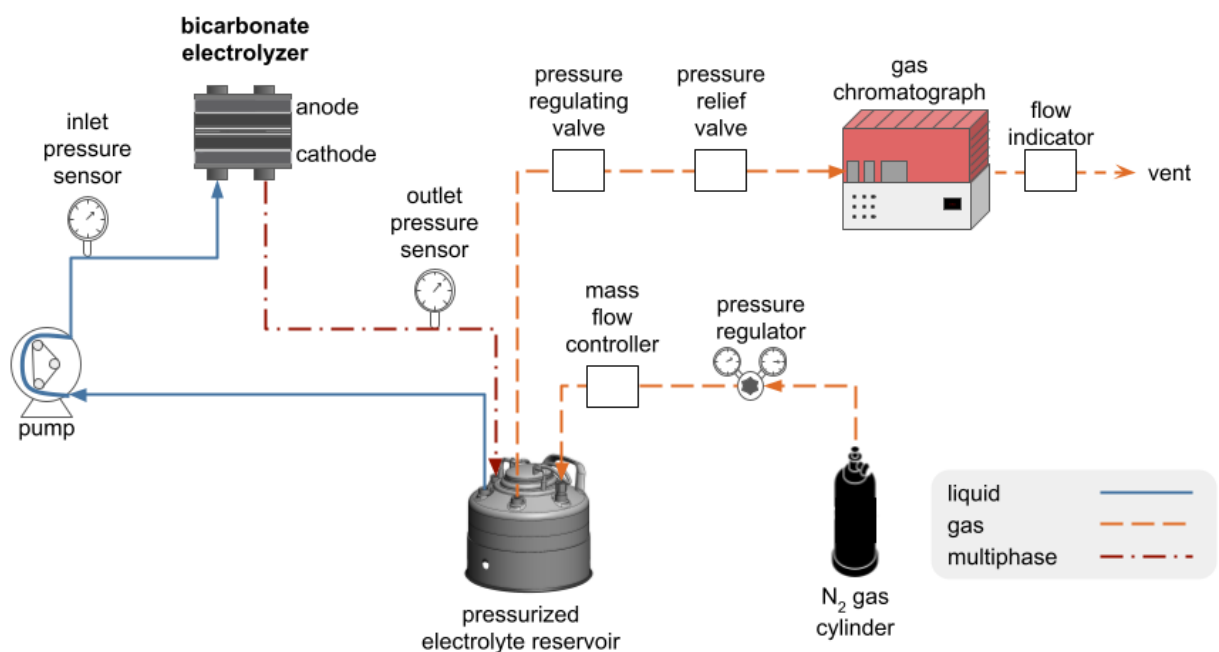
Figure S8. Schematic depiction of the pressurized bicarbonate electrolyser system. N$_2$ gas was used to control the pressure of the system, and the pressure value of the liquid feedstock was measured at the inlet of the electrolyser by a pressure sensor. The flow rate of gas was controlled using a mass flow controller and the pressure was controlled using a pressure regulating valve. The final products were measured by a gas chromatography. No liquid CO2RR product was detected.
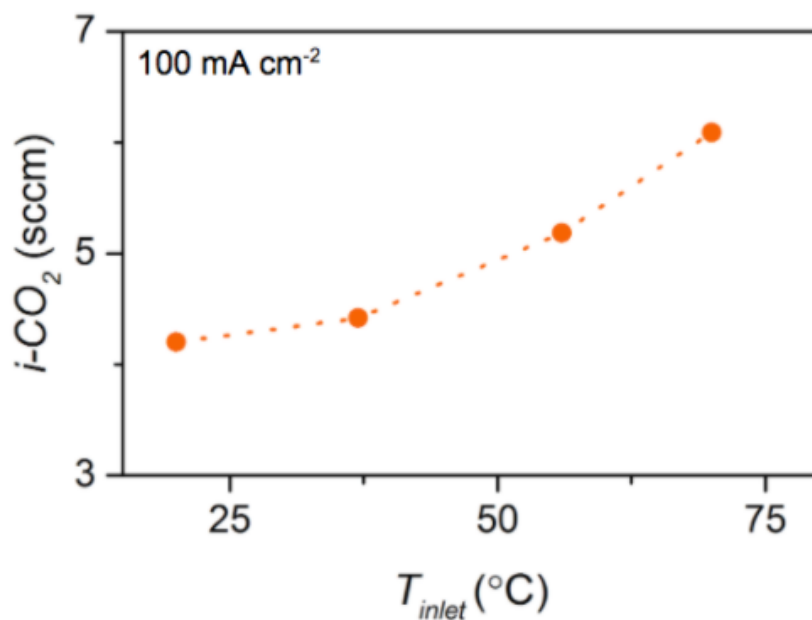
Figure S9. $i\text{-}CO_2$ flow rates measured in the outlet stream of the reactor during operation at a constant current density of 100 mA cm^{-2} for the silver foam electrode at different temperatures.
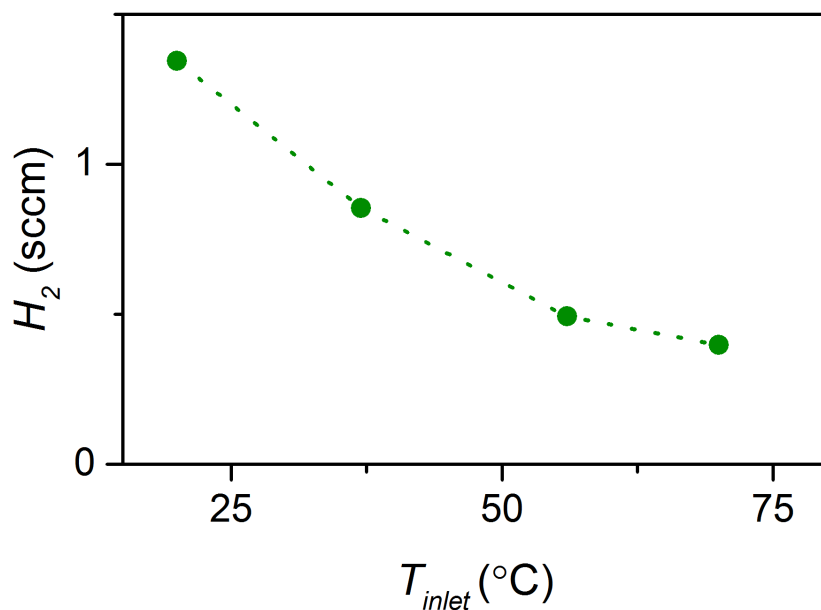
Figure S10. H_2 flow rates measured in the outlet stream of the reactor during operation at a constant current density of 100 mA cm^{-2} for the silver foam electrode at different temperatures.

(a)

(b)
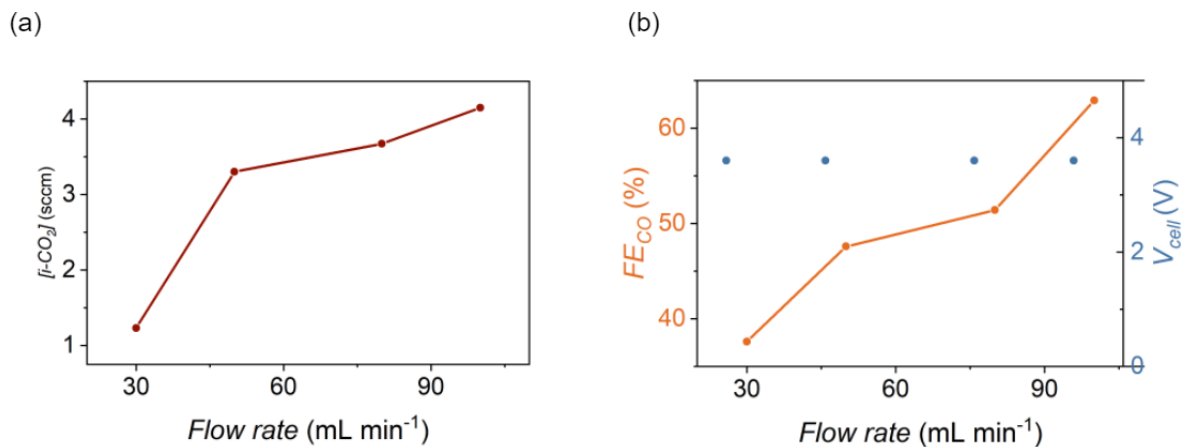
Figure S11. (a) *i*-CO_2 flow rates and (b) FE_{CO} and V_{cell} as a function of flow rates measured in the reactor during operation at a constant current density of 100 mA cm^{-2} for the silver foam electrode at different bicarbonate flow rates.

interdigitated flowplate   serpentine flowplate   parallel flowplate

silver
paint

2 cm

2 cm
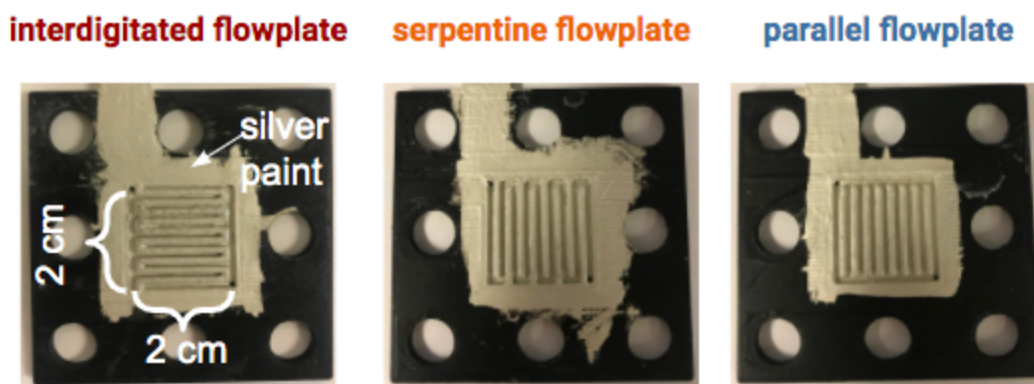
Figure S12. Photos of the 3D printed interdigitated, serpentine and parallel flow plates. Silver paint was used to make the flowplate conductive.
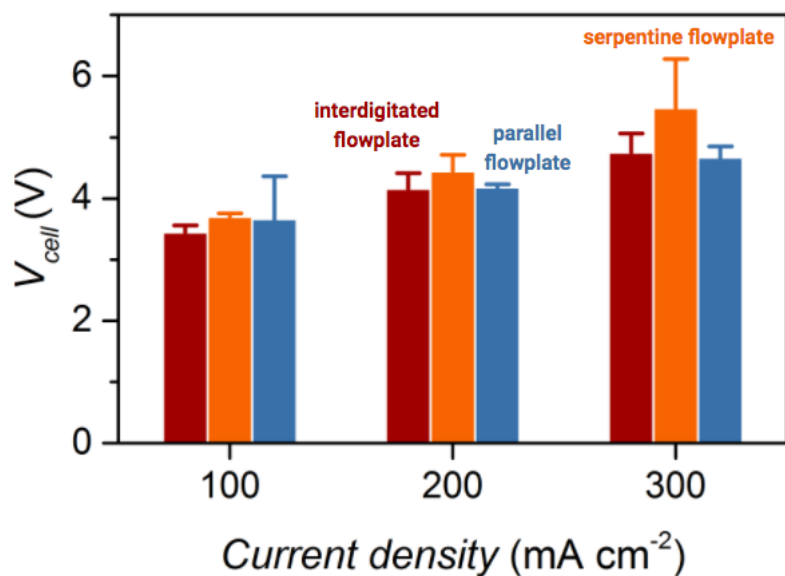
Figure S13. Cell voltages at varying current densities for the interdigitated, serpentine, and parallel flow patterns. Error bars denote the standard deviation of three replicated experiments.
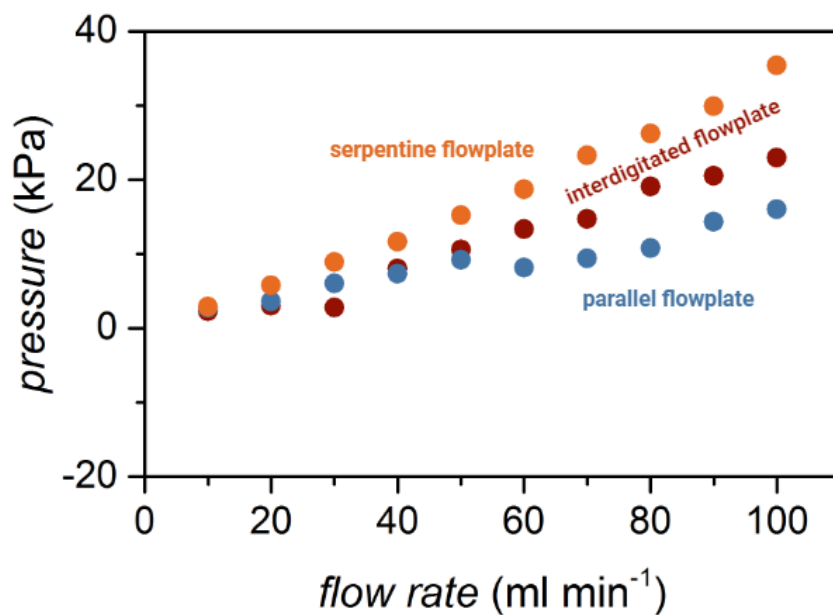
Figure S14. Comparison of inlet-to-outlet pressure drop for interdigitated, serpentine, and parallel flow pattern geometries.
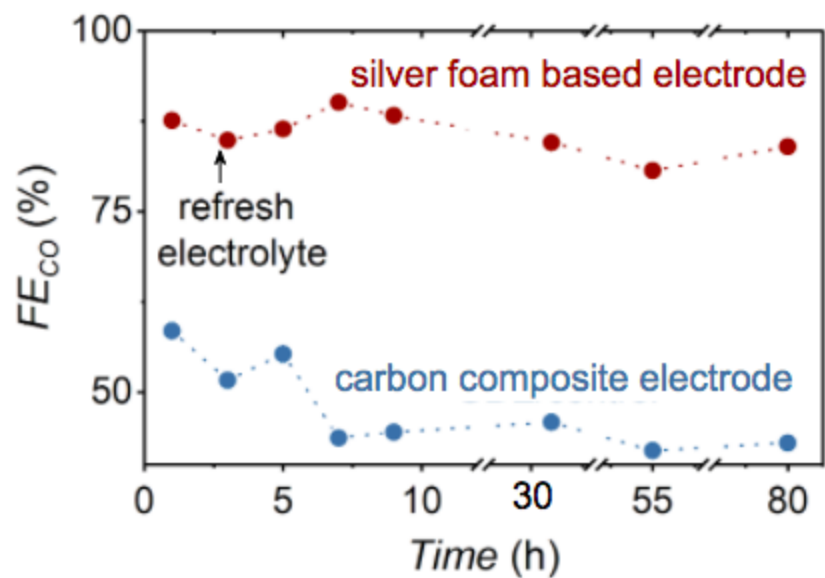
Figure S15. FE_{CO} at a constant applied current density of 65 mA cm^{-2} (20 °C, 1 atm) for 80 h for the silver foam and carbon composite electrodes.
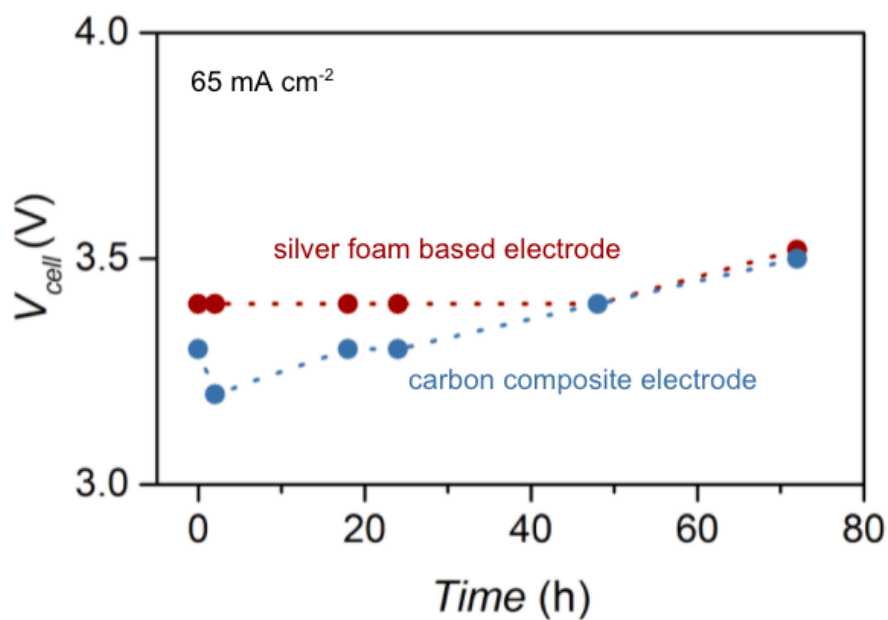
Figure S16. V_{cell} values measured during electrolyser stability tests at 65 mA cm^{-2} with the foam and carbon composite electrodes.
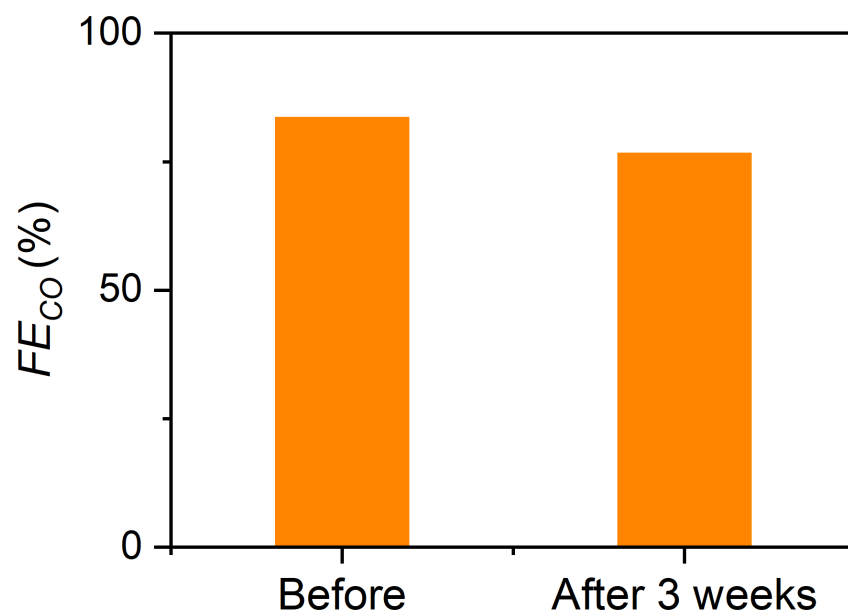
Figure S17. The silver foam electrode used for 80 h in the durability test was stored in air for 3 weeks, and FE_{CO} slightly decreased to 77% from 84% (65 mA cm^{-2}). The cell voltage was 3.8 V for the initial test and 3.6 V after 3 weeks.
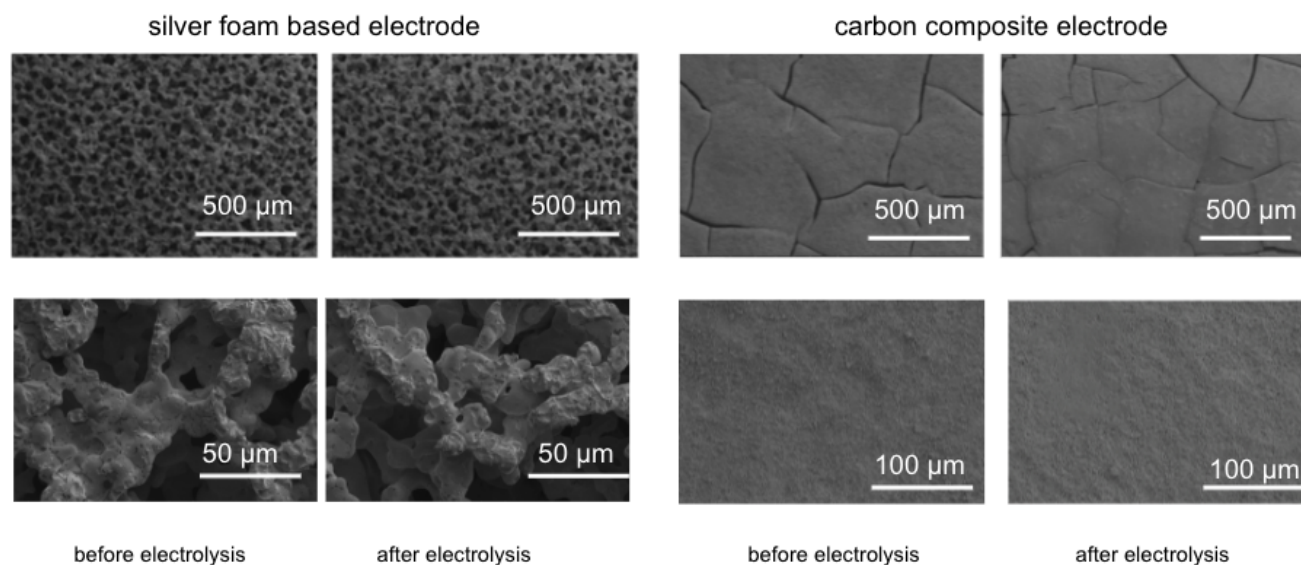
Figure S18. SEM images of the silver foam based electrode and carbon composite electrode taken before and after 80 h of electrolysis at 65 mA cm^{-2}.
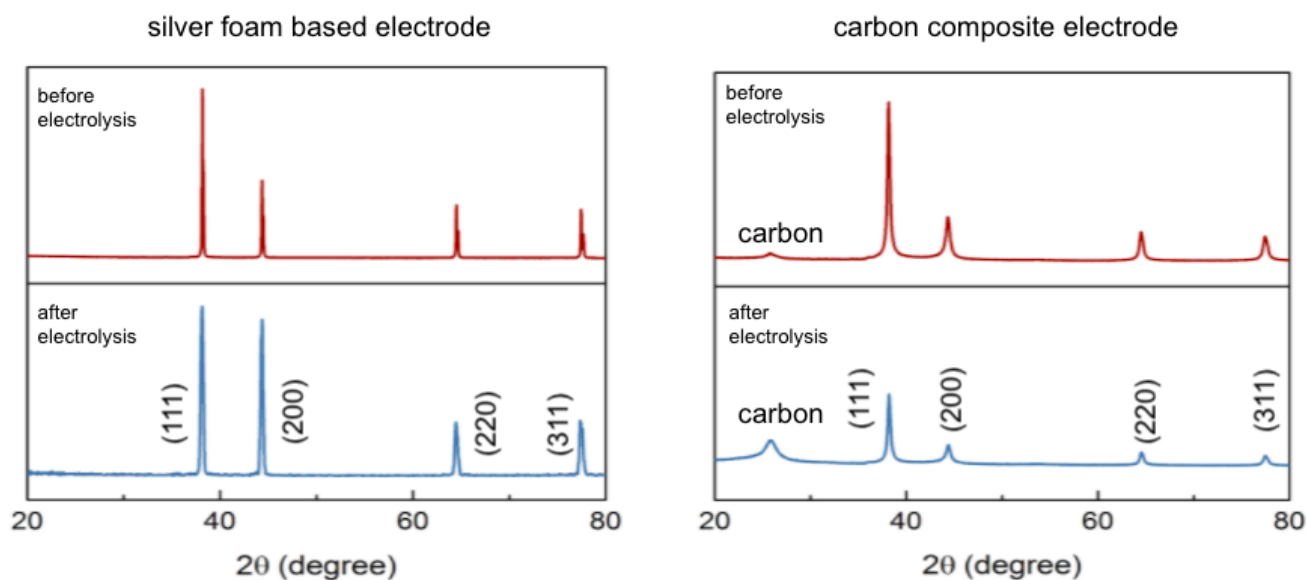
Figure S19. XRD spectra for the silver foam based electrode and carbon composite electrode before and after 80 h of electrolysis at 65 mA cm^{-2}.

References

1   J. He, A. Huang, N. J. J. Johnson, K. E. Dettelbach, D. M. Weekes, Y. Cao and C. P. Berlinguette, *Inorg. Chem.*, 2018, **57**, 14624–14631.

2   J. Choi, J. Kim, P. Wagner, S. Gambhir, R. Jalili, S. Byun, S. Sayyar, Y. M. Lee, D. R. MacFarlane, G. G. Wallace and D. L. Officer, *Energy Environ. Sci.*, 2019, 12, 747–755.

3   E. L. Clark, J. Resasco, A. Landers, J. Lin, L.-T. Chung, A. Walton, C. Hahn, T. F. Jaramillo and A. T. Bell, *ACS Catal.*, 2018, **8**, 6560–6570.

4   S. Oh, H. Kim, Y. Kwon, M. Kim, E. Cho and H. Kwon, *J. Mater. Chem. A Mater. Energy Sustain.*, 2016, **4**, 18272–18277.

5   D. A. Salvatore, D. M. Weekes, J. He, K. E. Dettelbach, Y. C. Li, T. E. Mallouk and C. P. Berlinguette, *ACS Energy Lett.*, 2018, **3**, 149–154.

6   H.-R. 'molly' Jhong, S. Ma and P. J. A. Kenis, *Curr. Opin. Chem. Eng.*, 2013, **2**, 191–199.

7   M. Liu, X.-A. Mao, C. Ye, H. Huang, J. K. Nicholson and J. C. Lindon, *J. Magn. Reson.*, 1998, **132**, 125–129.

8   L.-C. Weng, A. T. Bell and A. Z. Weber, *Phys. Chem. Chem. Phys.*, 2018, **20**, 16973–16984.

9   E. W. Lees, M. Goldman, A. G. Fink, D. J. Dvorak, D. A. Salvatore, Z. Zhang, N. W. X. Loo and C. P. Berlinguette, *ACS Energy Letters*, 2020, 2165–2173.

10 R. B. Kutz, Q. Chen, H. Yang, S. D. Sajjad, Z. Liu and I. Richard Masel, *Energy Technology*, 2017, 5, 929–936.

11 Y. C. Li, D. Zhou, Z. Yan, R. H. Gonçalves, D. A. Salvatore, C. P. Berlinguette and T. E. Mallouk, *ACS Energy Lett.*, 2016, **1**, 1149–1153.

12 S. Ren, D. Joulié, D. Salvatore, K. Torbensen, M. Wang, M. Robert and C. P. Berlinguette, *Science*, 2019, **365**, 367–369.

13 S. Verma, Y. Hamasaki, C. Kim, W. Huang, S. Lu, H.-R. M. Jhong, A. A. Gewirth, T. Fujigaya, N. Nakashima and P. J. A. Kenis, *ACS Energy Lett.*, 2018, **3**, 193–198.

14 L. A. Diaz, N. Gao, B. Adhikari, T. E. Lister, E. J. Dufek and A. D. Wilson, *Green Chemistry*, 2018, 20, 620–626.

15 E. J. Dufek, T. E. Lister, S. G. Stone and M. E. McIlwain, *Journal of The Electrochemical Society*, 2012, **159**, F514–F517.

16   C. Delacourt, P. L. Ridgway, J. B. Kerr and J. Newman, *Journal of The Electrochemical Society*, 2008, **155**, B42.

17   T. Li, E. W. Lees, M. Goldman, D. A. Salvatore, D. M. Weekes and C. P. Berlinguette, *Joule*, 2019, **3**, 1487–1497.

18   W. Zhao, K. Huang, Q. Zhang, H. Wu, L. Gu, K. Yao, Y. Shen and Y. Shao, *Nano Energy*, 2019, **58**, 69–77.